Detailed Dynamics of the Nonradiative Deactivation of Adenine: A Semiclassical Dynamics Study

Yibo Lei,[†,‡] Shuai Yuan,[†,‡] Yusheng Dou,[*,‡,§] Yubin Wang,[†] and Zhenyi Wen[†,‡]

Institute of Modern Physics, Northwest University, Xi'an, Shaanxi, 710069, P. R. China, Institute of Computational Chemistry, Chongqing University of Posts and Telecommunications, Chongqing, 400065, P. R. China, and, Department of Physical Sciences, Nicholls State University, PO Box 2022, Thibodaux, Louisiana 70310

Received: March 19, 2008; Revised Manuscript Received: June 10, 2008

A realistic dynamics simulation study is reported for the ultrafast radiationless deactivation of 9H-adenine. The simulation follows two different excitations induced by two 80 fs (fwhm) laser pulses that are different in energy: one has a photon energy of 5.0 eV, and the other has a photon energy of 4.8 eV. The simulation shows that the excited molecule decays to the electronic ground state from the $^1\pi\pi^*$ state in both excitations but through two different radiationless pathways: in the 5.0 eV excitation, the decay channel involves the out-of-plane vibration of the amino group, whereas in the 4.8 eV excitation, the decay strongly associates with the deformation of the pyrimidine at the C_2 atom. The lifetime of the $^1n\pi^*$ state determined in the simulation study is 630 fs for the 5.0 eV excitation and 1120 fs for the 4.8 eV excitation. These are consistent with the experimental values of 750 and 1000 fs. We conclude that the experimentally observed difference in the lifetime of the $^1n\pi^*$ state at various excitations results from the different radiationless deactivation pathways of the excited molecule to the electronic ground state.

1. Introduction

The high photostability of DNA as a primary UV chromophore of the genetic material of life is attributed to the presence of ultrafast nonradiative deactivation pathways. Through the nonradiative deactivation, electrically excited nucleobases in DNA decay to the vibrationally excited ground state on a subpicosecond time scale. The fast internal conversion prevents the destruction of DNA.[1,2]

Adenine is one of most important nucleobases in DNA and 9H-adenine, shown in Figure 1, is the most stable tautomer.[3] Numerous experimental investigations have been performed to characterize the ultrafast radiationless deactivation of 9H-adenine in gas phase. The electronic spectroscpy study by Kim and coworkers[4] showed that the lowest electronically excited state is $^1n\pi^*$, and the$^1\pi\pi^*$ state lies only about 600 cm^{-1} above the $^1n\pi^*$state. These two states are therefore considered to be mixed with each other in the FC region. Some other low-lying excited states were also identified by vibronically resolved spectroscopy investigations.[5−8] The lifetimes of the$^1\pi\pi^*$ and $^1n\pi^*$ states, when excited by a laser beam of 267 nm, were found to be 100 fs and 1 ps, respectively.[9−11] Recent femtosecond time-resolved photoelectron spectroscopy study showed[12−14] that the lifetime of the $^1\pi\pi^*$ state decreases to less than 50 fs if a laser energy of 250 nm is used. Similarly, the lifetime of the $^1n\pi^*$ state changes from 2.3 ps to less than 1.0 ps if the laser energy varies from 272 to 250 nm.[12−14] It was also found that the amplitude of the$^1n\pi^*$ state decreases significantly at the higher excitation energies.[14]

To understand the mechanisms of the ultrafast radiationless deactivation of excited adenine, various high-level quantum calculations have been carried out, including DFT-MRCI,[15,16] CASPT2/CASSCF,[17−27] and other approximations.[28,29] The theoretical investigations have proposed three different pathways for the radiationless decay of the electronically excited states. All three pathways rely on the internal conversion through conical intersections. The first kind of path is associated with the out-of-plane deformation of the pyrimidine ring in 9H-adenine. This mechanism assumes that out-of-plane vibrational modes of the pyrimidine ring play a central role in the formation of the conical intersection between the $^1\pi\pi^*$ state and the electronic ground state (denoted by $^1\pi^2$). A typical vibrational mode involved in this conical intersection is the ring-puckering vibration at the C_2 site. The second mechanism is based on the fact that the out-of-plane vibrational mode of the amino group is responsible for the conical intersection between the$^1n\pi^*$ and $^1\pi^2$ states. Another often-discussed mechanism is associated with an excited state $^1\pi\sigma^*$ located at the N_9-H position. The σ here is an antibonding Rydbergy-like orbital. This mechanism proposes that the large-amplitude motion of this hydrogen atom leads to a crossing between the $^1\pi\sigma^*$ state and the electronic

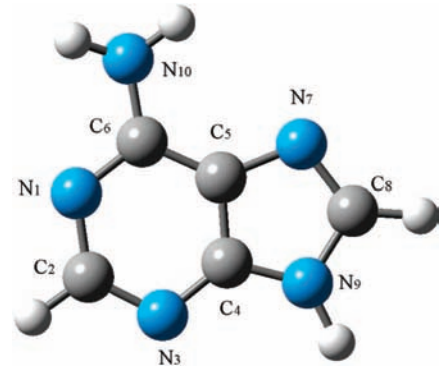

Figure 1. Structure and standard numbering of 9H-adenine.

* Corresponding author. Fax: 985 448 4927. E-mail: Yusheng.Dou@nicholls.edu.
† Northwest University.
‡ Chongqing University of Posts and Telecommunications.
§ Nicholls State University.

10.1021/jp802483b CCC: $40.75
Published on Web 08/21/2008

ground state. Although both experimental evidence and theoretical calculations suggest the existence of the $^1\pi\sigma^*$ channel, it may not play a significant role because it cannot explain the photostability of DNA in which a deoxyribose group is attached at the N_9 site. Nevertheless, each of these mechanisms needs further investigations.

Theoretical investigations on the photostability of 9H-adenine typically use static quantum calculations to locate the energy minimum on the potential energy surfaces and search the minimum-energy path by connecting the critical points. These calculations are fundamental in understanding the main features of the mechanisms behind the ultrafast radiationless deactivation. However, the static calculations alone cannot provide detailed information for a specific reaction path that is actually realized in a deactivation course because of the following limitations: (1) they are incapable of describing the time-dependent properties of the deactivation process, (2) they are usually performed along one or two reaction coordinates with other coordinates fixed and consequently are insufficient in characterizing a real deactivation process where all reaction coordinates are involved and play a non-negligible role, and (3) they do not include the laser pulse properties and subsequently cannot provide detailed explanations for photochemical experiments in which the laser pulse parameters strongly influence the reaction.

In this work, we study the dynamics of the radiationless deactivation of the low-lying excited states of 9H-adenine following the excitation by different laser pulses by a semiclassical dynamics simulation approach. In our simulation study, all degrees of freedom of the molecule are included in the calculations and the laser pulse is explicitly coupled to electrons. By monitoring the nuclear motions triggered by a specific laser pulse, we are able to describe a realistic deactivation path. Examining the interplay of the electronic and nuclear motions allows one to study the influence of different vibrational modes on the radiationless deactivation process of the excited molecule. The simulation results presented in this publication provide complementary information for understanding the mechanisms of the radiationless deactivation of excited 9H-adenine.

2. Methodology

In our semiclassical dynamics simulation approach, the state of the valence electrons is calculated by the time-dependent Schrödinger equation, but the radiation field and the motion of the nuclei are treated classically.

A detailed description of this method has been published elsewhere;[30,31] therefore, only a brief explanation is presented here. The time-dependent Schrödinger equation is solved at each time step in a nonorthogonal basis to produce the one-electron states,

$$i\hbar\frac{\partial \mathbf{\Psi}_j}{\partial t} = \mathbf{S^{-1}} \cdot \mathbf{H} \cdot \mathbf{\Psi}_j \tag{1}$$

where $\mathbf{S}$ is the overlap matrix for the atomic orbitals. This equation is solved by using a unitary algorithm obtained from the equation for the time evolution operator.[32]

The laser pulse is characterized by the vector potential $\mathbf{A}$ and is coupled to the Hamiltonian through the time-dependent Peierls substitution[33,34]

$$H_{ab}(\mathbf{X}-\mathbf{X}') = H^0_{ab}(\mathbf{X}-\mathbf{X}')\exp\left(\frac{iq}{\hbar c}\mathbf{A}\cdot(\mathbf{X}-\mathbf{X}')\right) \tag{2}$$

Here, $H_{ab}(\mathbf{X}-\mathbf{X}')$ is the Hamiltonian matrix element for basis functions a and b on atoms at $\mathbf{X}$ and $\mathbf{X}'$, respectively, and $q = -e$ is the charge of the electron.

In our previous investigations, this same model was found to yield good descriptions of molecular response to ultrashort laser pulses. This includes that the explanation of the nonthermal fragmentation of C_{60}[35] is in good agreement with experimental observations,[36] the simulation of the formation of the tetramethylene intermediate diradical[37] is consistent with the time-of-flight mass spectrometry measurement,[38] and the characterization of the geometry changes at some critical points[39] is compatible with the molecular mechanics valence bond calculations.[40]

The electronic structure in the present simulation is calculated by a density-functional-based tight-binding method (DFTB).[41] The electronic energy of the system can be approximately written as

$$E_{\text{elec}} = \sum_{i=\text{occ}} n_i\varepsilon_i + \sum_{\alpha>\beta} U_{\text{rep}}(|X_\alpha - X_\beta|) \tag{3}$$

where the first sum is over the occupied orbitals, ε_i is eigenvalues of orbitals i and determined by solving Kohn−Sham equations, and n_i is the occupation number of orbital i. The effective repulsion potential $U_{\text{rep}}(|X_\alpha - X_\beta|)$ is the function of interatom distance.

The nuclear motion is solved by the Ehrenfest equation of motion

$$\begin{aligned} M_l\frac{\mathrm{d}^2X_{l\alpha}}{\mathrm{d}t^2} &= -\frac{\partial E_{\text{elec}}}{\partial X_{l\alpha}} \\ &= -\frac{1}{2}\sum_j \mathbf{\Psi}_j^+ \cdot \left(\frac{\partial \mathbf{H}}{\partial X_{l\alpha}} - i\hbar\frac{1}{2}\frac{\partial \mathbf{S}}{\partial X_{l\alpha}}\cdot\frac{\partial}{\partial t}\right)\cdot\mathbf{\Psi}_j - \\ &\quad \partial U_{\text{rep}}/\partial X_{l\alpha} \end{aligned} \tag{4}$$

where $X_{l\alpha} = \langle\hat{X}_{l\alpha}\rangle$ is the expectation value of the time-dependent Heisenberg operator for the α coordinate of the nucleus labeled by l (with $\alpha = x, y, z$). This equation is obtained by neglecting the terms of second and higher order in the quantum fluctuations $\hat{X} - \langle\hat{X}_{l\alpha}\rangle$ in the exact Ehrenfest theorem. This equation is numerically integrated with the velocity Verlet algorithm (which preserves phase space). A time step of 50 as was used on the basis of the test of energy conservation.

The present Ehrenfest approach is complementary to other methods based on different approximations. Its weakness is that it amounts to averaging over all the terms in the Born−Oppenheimer expansion[42−46]

$$\Psi^{\text{total}}(X_{\text{n}}, x_{\text{e}}, t) = \sum_i \Psi^{\text{n}}_i(X_{\text{n}}, t)\,\Psi^{\text{e}}_i(x_{\text{e}}, X_{\text{n}}, t) \tag{5}$$

rather than following the time evolution of a single term, that is, a single potential energy surface, which is approximately decoupled from all the others. (Here, X_{n} and x_{e} represent the sets of nuclear and electronic coordinates, respectively, and the Ψ^{e}_i are eigenstates of the electronic Hamiltonian at fixed X_{n}.) The present approach has the following strengths: it retains all of the $3N$ nuclear degrees of freedom (instead of only the two or three that are typically considered in a potential-energy-surface calculation), and it includes both the excitation due to a laser pulse and the subsequent de-excitation at an avoided crossing or a conical intersection[32,44−48]

3. Results and Discussion

3.1. Optimized Ground-State Geometry. The ground-state geometry of 9H-adenine is obtained after a 1000 fs simulation. The molecule has a planar structure, and the geometry parameters, including the bond lengths, bond angles, and dihedral

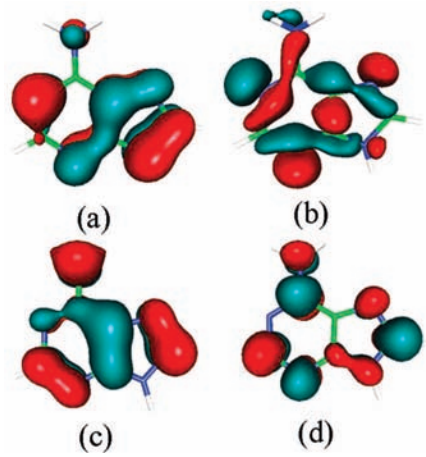

Figure 2. Molecular orbitals (a) HOMO-2, (b) HOMO-1, (c) HOMO, and (d) LUMO of 9H-adenine at $t = 0$ fs.

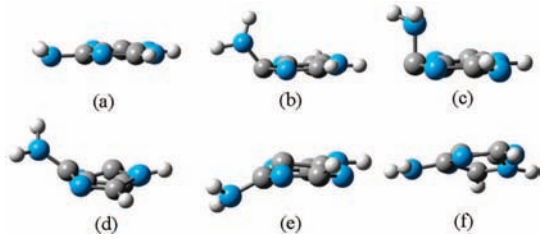

Figure 3. Snapshots taken at different times in a simulation of 9H-adenine in response to excitation by a 80 fs (fwhm) laser pulse with a fluence of 0.229 kJ/m^2 and photon energy of 5.0 eV. (a−f) are at 0, 800, 1030, 1120, 1200, and 1400 fs, respectively.

angles as well as energies are found to be in good agreement with published results.[24] Four molecular orbitals, namely, the HOMO-2, HOMO-1, HOMO, and LUMO, are plotted in Figure 2. The HOMO-2 and HOMO are π orbitals, the LUMO is π^* orbital, and HOMO-1 is lone-pair orbital associated with nitrogen atoms in the purine moiety. The experimentally observed two low-lying states $^1\pi\pi^*$ and $^1n\pi^*$ can be described dominantly by HOMO → LUMO and HOMO-1 → LUMO transitions. These molecular orbitals play a central role in the laser excitations and de-excitation of the molecule.

3.2. Decay-Path via the Out-of-Plane Twist of the Amino Group. To produce an excited state, in which the out-of-plane vibration of 9H-adenine is appreciably activated, a 80 fs (fwhm) laser pulse was applied with an effective photon energy of 5.0 eV. The energy selected matches the energy gap between the HOMO-2 and LUMO in the present density-functional-based approach for the equilibrated ground-state geometry. Simulations were run for different fluences, but only representative results will be presented for a fluence of 0.229 kJ/m^2 that generates the desired vibrational motion.

Six snapshots from the simulation at different times are shown in Figure 3. Starting from the equilibrium geometry in the electronic ground-state at 0 fs, the 9H-adenine molecule is electronically excited by the laser pulse. The most impressive features of the nuclear motions of the excited molecule are the out-of-plane vibration of the amino group and the deformation of the pyrimidine ring at the C_6 atom.

The variations of the $C_6-C_5-C_4-N_9$ and $N_3-C_4-C_5-N_7$, and $C_4-C_5-C_6-N_{10}$ dihedral angles with time are plotted in Figure 4. Both the $C_6-C_5-C_4-N_9$ and $N_3-C_4-C_5-N_7$ dihedral angles oscillate slightly about their initial value of 180°, although the amplitudes of these vibrations are somewhat greater after 1100 fs. This suggests that the molecule remains roughly a

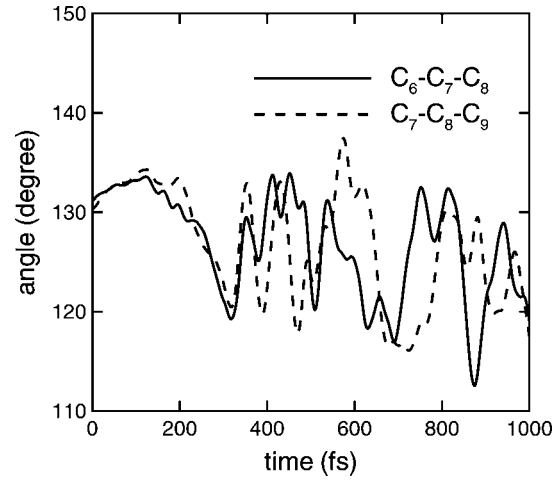

Figure 4. Changes in (a) the $C_6-C_5-C_4-N_9$ and $C_3-C_4-C_5-N_7$ and (b) the $C_4-C_5-C_6-N_{10}$ dihedral angles of 9H-adenine subjected excitation by a 80 fs (fwhm) laser pulse with a fluence of of 0.229 kJ/m^2 and photon energy of 5.0 eV.

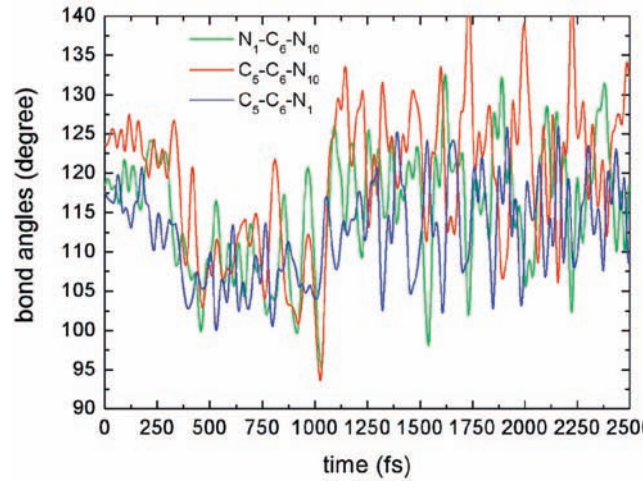

Figure 5. Variation with time of the $N_1-C_6-N_{10}$, $C_5-C_6-N_{10}$, and $C_5-C_6-N_1$ bond angles of 9H-adenine subjected a 80 fs (fwhm) laser pulse with a fluence of of 0.229 kJ/m^2 and photon energy of 5.0 eV.

planar geometry for this excitation. On the other hand, as can be viewed in Figure 4b, the $C_4-C_5-C_6-N_{10}$ dihedral angle decreases gradually from 180° to about 82° at 1034 fs and then increase quickly to 270° by 1333 fs. After this time, the dihedral angle decreases again. The out-of-plane vibration of the amino group in the pyrimidine ring can be reasonably presented by the changes with time in the $C_4-C_5-C_6-N_{10}$ torsional angle. Figure 4b demonstrates that when excited by the 5.0 eV laser pulse, the amino group takes an out-of-plane vibration. It becomes approximately perpendicular to the pyrimidine ring at 1030 fs and then swings back.

Although all bond angles change to response to the laser excitations, three angles, namely, $N_1-C_6-N_{10}$, $C_5-C_6-N_{10}$, and $C_5-C_6-N_1$, show the most notable variations due to the laser excitation. Figure 5 demonstrates the variations of these angles with time. Figure 5 shows that before 300 fs, these three bond angles vibrate considerably about their elementary values, 118° for $N_1-C_6-N_{10}$, 117° for $C_5-C_6-N_1$, and 124° for $C_5-C_6-N_{10}$. Shortly after 300 fs, the three bond angles are compressed and get shorter to an average value of 105° by 450 fs. They remain at this value as long as 1050 fs. The three bond angles finally expand to around their primary values and stay about these values over the rest of the simulation time. The

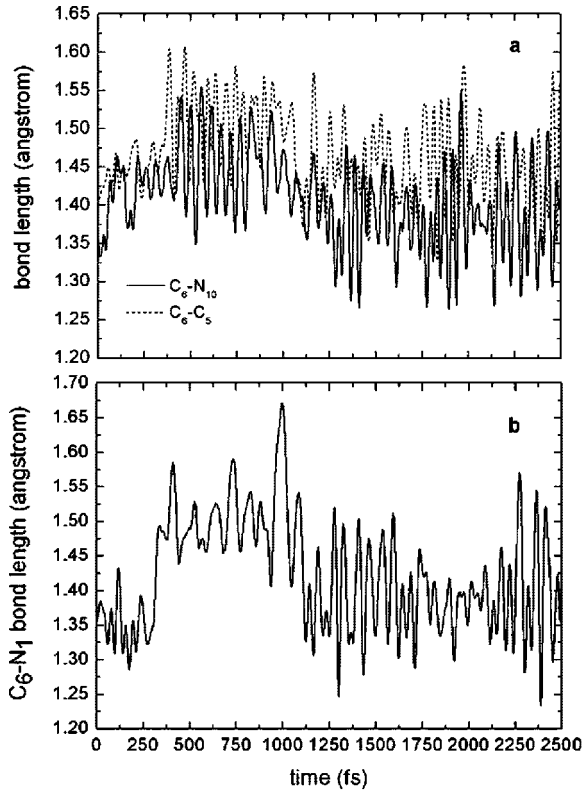

Figure 6. Changes with time of (a) the C_6-N_{10} and C_6-C_5 and (b) the C_6-N_1 bonds of 9H-adenine excited by a 80 fs (fwhm) laser pulse with a fluence of of 0.229 kJ/m^2 and photon energy of 5.0 eV.

changes in these bond angles are closely related to the out-of-plane vibration of the amino group: the compression of the bond angles is concurrent with the increase in the displacement of the amino group from its equilibrium position.

Another substantial change in the molecular geometry associated with the out-of-plane vibration of the amino group is the lengths of bonds connecting to C_6 atom, including the C_6-N_{10}, C_6-N_1, and C_5-C_6 bonds. The variations with time of the lengths of these bonds are displayed in Figure 6a,b. The C_6-N_{10} bond stretches from 1.35 Å to an average value of 1.44 Å shortly after the laser excitation and then vibrates about this length before 1000 fs. The amplitude of the stretching vibration is conspicuously enhanced from 430 fs. After 1030 fs, it becomes shorter and comes back to its starting length at 1310 fs. The C_6-N_{10} bond then vibrates about this value for the rest of the simulation time. The C_5-C_6 bond, which has the starting length of 1.40 Å, demonstrates a variation trend with time similar to that of the C_6-N_{10} bond. On the other hand, the C_6-N_1 bond length slightly decreases from its original value of 1.37 Å in the first 300 fs. Soon after then, it quickly rises up to about 1.50 Å and fluctuates about this value until 1100 fs. It drops back to its basic value after 1100 fs.

The populations and energies of four interesting frontier molecular orbitals, including the HOMO-2, HOMO-1, HOMO, and LUMO, are shown in Figures 7 and 8. An expanded scale of the orbital populations from 0 to 160 fs is plotted in Figure 7a for illustration. The excitations of electrons are primarily from the HOMO-2 to LUMO although other minor excitations, for example, from the HOMO-1 to LUMO, are noticeable. At the end of the laser pulse, 160 fs in full duration, the LUMO accommodates roughly 1.6 electrons, and the HOMO-2 has lost approximately 0.9 electrons or holds about 0.9 holes. The variations of the electronic populations in different molecular

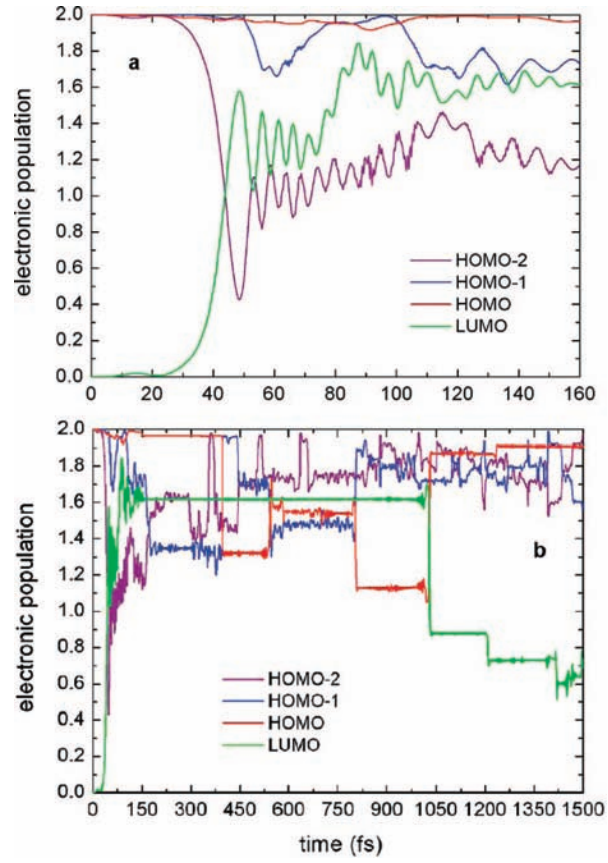

Figure 7. Variation with time of the electronic populations of the HOMO-2, HOMO-1, HOMO, and LUMO (a) from 0 to 160 fs and (b) from 0 to 1500 fs, following application of a 80 fs (fwhm) laser pulse with a fluence of 0.229 kJ/m^2 and a photon energy of 5.0 eV.

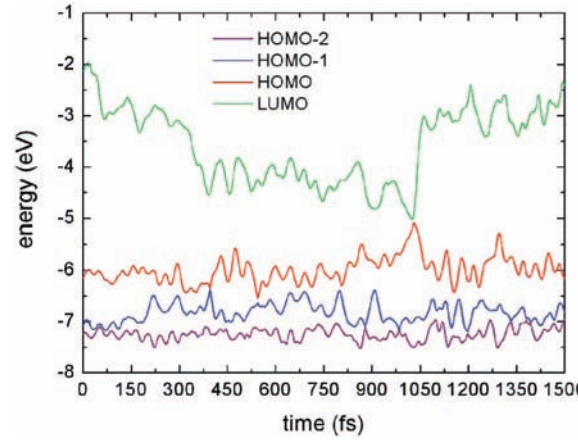

Figure 8. Energy variation with time of the HOMO-2, HOMO-1, HOMO, and LUMO, following application of a 80 fs (fwhm) laser pulse with a fluence of 0.229 kJ/m^2 and a photon energy of 5.0 eV.

orbitals induce the changes in the forces on the nuclei, driving them into motion. Many vibration modes of the molecule, including the dihedral motions, bond bending vibrations, and bond stretch vibrations, are excited. These excitations in turn change the gaps between the different molecular orbitals.

After the completion of the laser pulse, several significant electronic transfers arise between the HOMO-2 and HOMO-1 and the HOMO-1 and HOMO which can be observed through population changes around close proximity between two related orbitals. The first event, which occurred at about 170 fs, transfers about 0.4 holes from the HOMO-2 to HOMO-1. The second

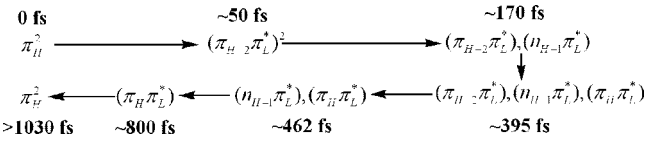

Figure 9. Summary of the electronic transitions presented in Figure 7. Please note that we interpret, for example, the electronic transition $\pi_{H-2} \rightarrow \pi_L^*$ and hole transition $\pi_{H-2} \rightarrow n_{H-1}$ as the electronic transition $n_{H-1} \rightarrow \pi_L^*$.

electron transfer, which remarkably appeared at 390 fs, brings about 0.55 holes from the HOMO-1 to HOMO. A sudden stretching of the C_5-C_6 bond at 390 fs and notable enlargement of the amplitude of the stretching vibration immediately after then, as see in Figure 6a, indicates that the C_5-C_6 bond stretching vibration is involved in this nonadiabatic transition. At 800 fs, about 0.5 holes are shifted from the HOMO-1 to HOMO. As can be seen in Figure 5, at this time, the $C_5-C_6-N_{10}$ bond angle significantly expands, and the amplitude of the $C_5-C_6-N_{10}$ angle bending vibration gains a considerable increase, suggesting that the $C_5-C_6-N_{10}$ angle bending motion is greatly involved in this coupling.

The molecule finally eventually decays to the electronic ground state because the de-excitation of electrons from the LUMO to HOMO occurred at 1050 fs when the energies of two orbitals are in close proximity to each other, as seen in Figures 7b and 8. The accompaniment of this nonadiabatic transition with a fast switch of the amino group back to its equilibrium position from its perpendicular position to the pyrimidine ring, as shown in Figure 4b, suggests that the out-of-plane vibration is the main component responsible for the vibronic coupling between the HOMO−LUMO, through which 9-H adenine de-excites to the electronic ground state.

The electronic transitions HOMO-2 → LUMO, HOMO-1 → LUMOm and HOMO → LUMO can also be denoted as $\pi_{H-2}\pi^*$, $n_{H-1}\pi^*$, and $\pi_H\pi^*$, respectively. The electronic events found in Figure 7 are summarized in Figure 9 by using the new nomenclature. This allows estimating the lifetime of an electronically excited state which has a dominant transition found in Figure 7. For example, the electronic state ruled by the $n_{H-1}\pi^*$ configuration, which appears at 170 fs and extinguishes at 800 fs, has a lifetime of 630 fs.

3.3. Decay-Path Involving the Out-of-Plane Twist of the C_2-H Bond. A laser pulse of 80 fs (fwhm) with an effective photon energy of 4.8 eV was applied to generate an excitation of 9H-adenine, in which the C_2H puckering vibration is impressively excited. The photon energy selected corresponds to the energy difference between the HOMO-1 and LUMO for the beginning ground-state geometry of the molecule in the present approximation. Again, the simulations were run for various fluences, and only one typical trajectory will be examined for a fluence of 0.384 kJ/m^2 that creates the desired vibration mode.

Six snapshots from the simulation at different times for this excitation are shown in Figure 10. The laser excitation starts at 0 fs and 9H-adenine becomes electronically excited after about 120 fs. The most impressive features showed in Figure 10 are the out-of-plane vibration of the H atom connected to the C_2 atom and the deformation of the pyrimidine ring at the C_2 site.

The variations with time of the $N_3-C_4-C_5-N_7$ and $C_6-C_5-C_4-N_9$ dihedral angles are plotted in Figure 11. Both torsional motions are conspicuously activated after 300 fs. The increase in the $N_3-C_4-C_5-N_7$ and decrease in the $C_6-C_5-C_4-N_9$ dihedral angles after 300 fs imply that the pyrimidine ring and imidazole ring are no longer coplaned. After 1400 fs, each dihedral angle comes back to its initial value on the average, and the molecule returns to its plane geometry. Figure 12 shows the changes in the $C_2-N_3-C_4-C_5$ and $C_4-N_3-C_2-H$ dihedral angles against time. The changes in the $C_2-N_3-C_4-C_5$ angle provide information on the deformation of the pyrimidine ring at the C_2 atom whereas the variations of the $C_4-N_3-C_2-H$ angle provide indications for the displacements of the H atom away from the pyrimidine ring. The four largest deformations

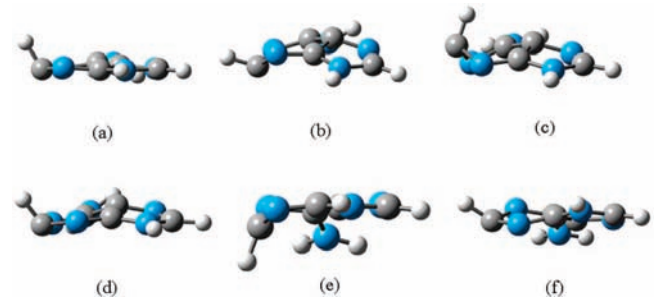

Figure 10. Snapshots taken at different times in a simulation of 9H-adenine excited by a 80 fs (fwhm) laser pulse with a fluence of 0.384 kJ/m^2 and a photon energy of 4.8 eV. (a−f) are at 232, 570, 745, 1200, 1329, and 1420 fs, respectively.

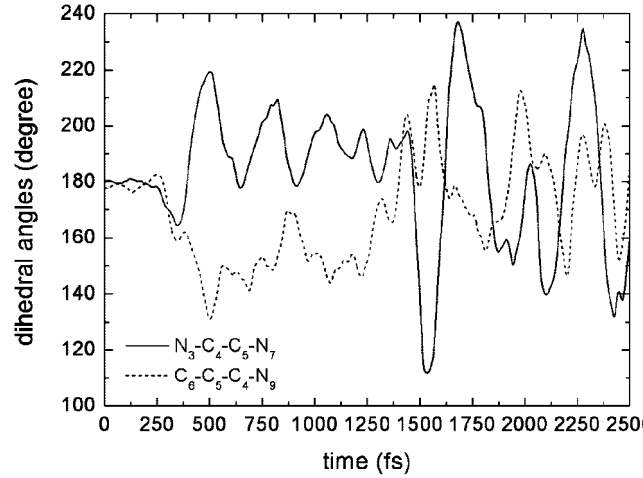

Figure 11. Variation with time of (a) the $C_6-C_5-C_4-N_9$ and $C_3-C_4-C_5-N_7$ dihedral angles and (b) the $C_4-C_5-C_6-N_{10}$ dihedral angle of 9H-adenine excited by a 80 fs (fwhm) laser pulse with a fluence of 0.384 kJ/m^2 and a photon energy of 4.8 eV.

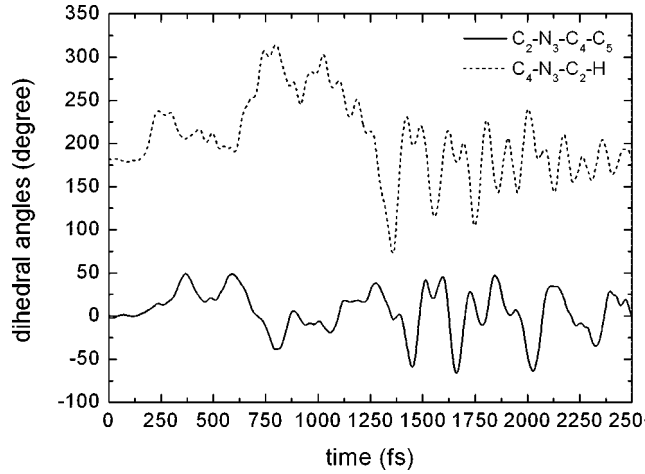

Figure 12. Changes in the $C_2-N_3-C_4-C_5$ and $C_4-N_3-C_2-H$ dihedral angles of 9H-adenine in responding to excitation by a 80 fs (fwhm) laser pulse with a fluence of 0.384 kJ/m^2 and a photon energy of 4.8 eV.

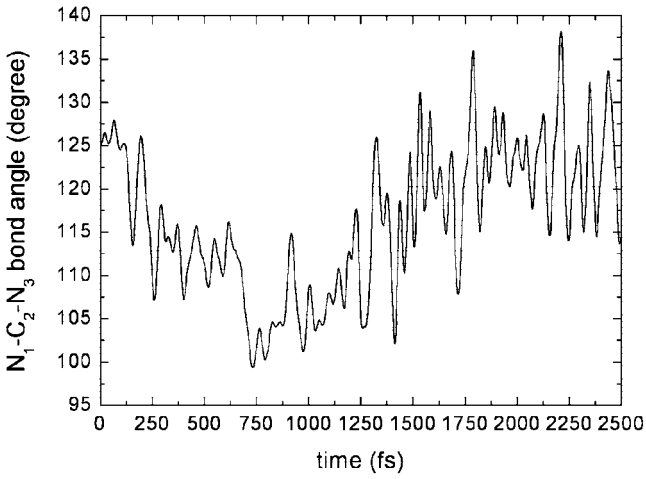

Figure 13. Changes in the $N_1-C_2-N_3$ and $C_4-C_5-C_6$ bond angles of 9H-adenine in responding to excitation by a 80 fs (fwhm) laser pulse with a fluence of 0.384 kJ/m^2 and a photon energy of 4.8 eV.

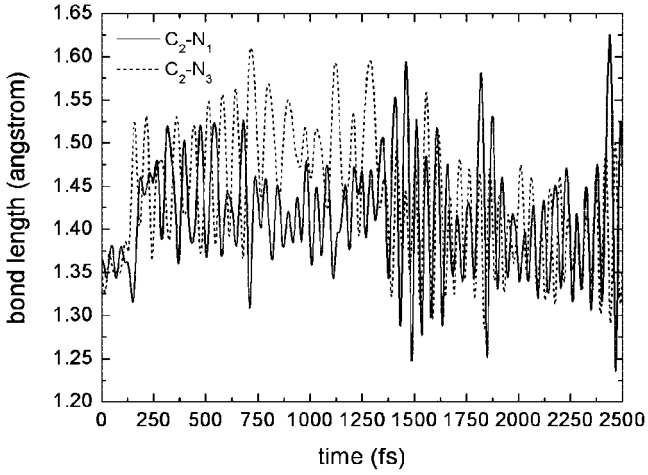

Figure 14. Time dependence of the C_2-N_1 and C_2-N_3 bonds of 9H-adenine in responding to excitation by a 80 fs (fwhm) laser pulse with a fluence of 0.384 kJ/m^2 and photon energy of 4.8 eV.

of the pyrimidine ring at the C_2 atom are observed at 380, 600, 810, and 1290 fs, and three extraordinary displacements of the H atom from its equilibrium positions are found at about 780, 1030, and 1360 fs. After 1400 fs, the H atom swings back to its fundamental position and oscillates about this position with a quite smaller period and greater amplitude, and the molecule vibrates about its equilibrium structure.

Among many bond angles, the $N_1-C_2-N_3$ angle exhibits the most noteworthy variations due to the laser excitation, as shown in Figure 13. These variations are directly associated with the C_2H puckering vibration, as see in Figure 12. The minimum of the bond angle amplitude coincides with the maximum of the displacement of the C_2 atom from its equilibrium position.

Two bond lengths, C_2-N_1 and C_2-N_3, demonstrate the most appreciable variations with time during the simulation time. These variations are plotted in Figure 14. The C_2-N_3 bond stretches from an initial value of 1.35 Å to 1.47 Å on average by 160 fs and then remains at this length until 1360 fs. Soon after this time, it shortens to a length less than 1.40 Å on average and keeps this length for the rest of the simulation time. The C_2-N_1 bond expands from a beginning value of 1.36 Å to 1.45 Å on average at 180 fs. The bond is compressed at about 700 fs and again at 1400 fs and finally becomes shorter than 1.40 Å in length.

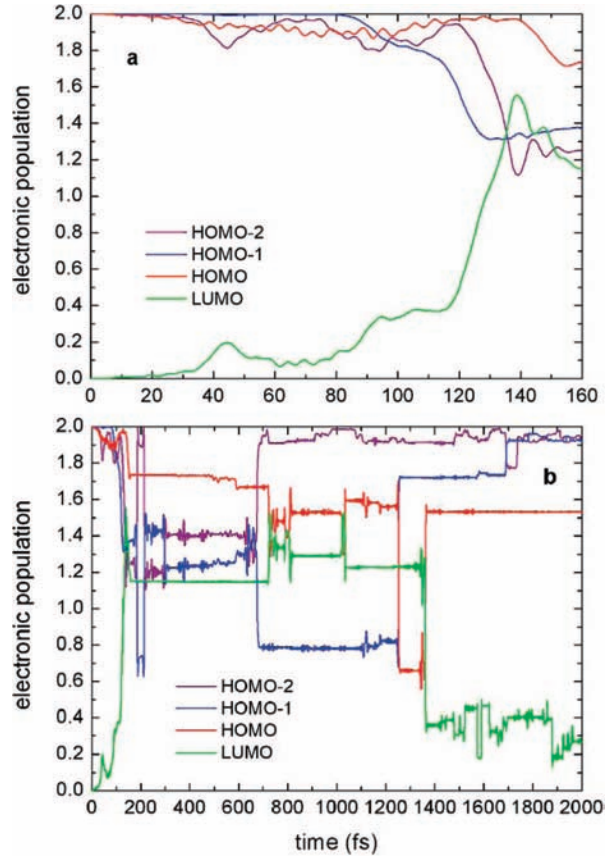

Figure 15. Variation with time of the electronic populations of the HOMO-2, HOMO-1, HOMO, and LUMO orbitals (a) from 0 to 160 fs and (b) from 0 to 2000 fs of 9H-adenine following application of a 80 fs (fwhm) laser pulse with a fluence of 0.384 kJ/m^2 and a photon energy of 4.8 eV.

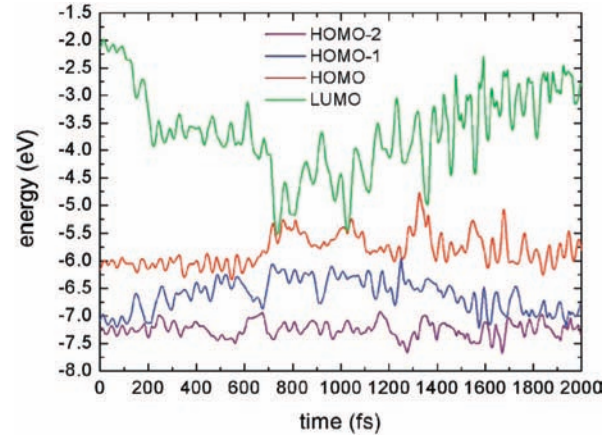

Figure 16. Energy variations with time of the HOMO-2, HOMO-1, HOMO, and LUMO of 9H-adenine following application of a 80 fs (fwhm) laser pulse with a fluence of 0.384 kJ/m^2 and a photon energy of 4.8 eV.

The populations and energies of the HOMO-2, HOMO-1, HOMO, and LUMO are presented in Figures 15 and 16. An expanded scale of the orbital populations from 0 to 160 fs is shown in Figure 15a. The laser pulse excites about 1.5 electrons to the LUMO and leaves the electronic holes mainly in the HOMO-2 and HOMO-1. There are also a small fraction of electrons in the higher-lying unoccupied orbitals and a small fraction of holes in the lower-lying occupied orbitals. However, they do not play a notable role in the dynamical process discussed below.

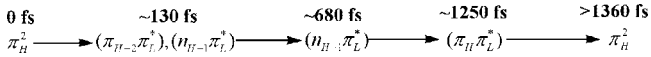

Figure 17. Summary of the electronic transitions presented in Figure 15. Please note that we interpret, for example, the electronic transition $\pi_{H-2} \rightarrow \pi_L^*$ and hole transition $\pi_{H-2} \rightarrow n_{H-1}$ as the electronic transition $n_{H-1} \rightarrow \pi_L^*$.

After the completion of the laser pulse, four electron transfers between the HOMO-2 and HOMO-1, which appeared at 187, 212, 297, and 640 fs, respectively, bring almost all holes in the HOMO-2 to the HOMO-1. These orbital population variations occur at the times when two orbitals are in close proximity to each other, as shown in Figure 16. About 0.9 holes are transferred from the HOMO-1 to HOMO at 1250 fs because these two orbitals are in close proximity to each other. Finally, the molecule returns to the electronic ground state through nonadiabatic transition at 1360 fs as a result of the depopulation of the LUMO when it very closely approaches to the HOMO in energy, as displayed in Figure 16. This process involves a large displacement of the C_2 atom from its equilibrium position and a strong deformation of the pyrimidine ring at the C_2 site, as seen in Figure 12a,b, and it is therefore concluded that the out-of-ring vibration of the H atom and the deformation of the pyrimidine ring resulted from the out-of-ring twist of the C_2H group are the main causes of the nonadiabatic transition leading the molecule to the ground state. Similarly, other two small energy gaps between the HOMO and LUMO at about 780 and 1030 fs also associate with the two largest displacements of the H atom from its equilibrium position.

The electronic events presented in Figure 15 are summarized in Figure 17, from which the lifetime of the $^1n\pi^*$ state is determined to be 1120 fs.

4. Conclusion

We have investigated the nonradiative deactivation of 9H-adenine by employing a realistic simulation approach that couples the dynamics of electrons and nuclei. The simulation follows two different excitations that lead to two altered ultrafast radiationless deactivation paths: path through the out-of-plane vibration of the amino group and the ring-puckering vibration of the C_2H group. The former path is induced by the laser pulse with 250 nm (5.0 eV) excitation, whereas the latter is induced by the laser pulse with 267 nm (4.8 eV) excitation. In both excitations, electrons are promoted to the LUMO from orbitals below the HOMO. In the former event, more electrons come from the HOMO-2 than from the HOMO-1. However, in the latter one, electrons are almost equally from the HOMO-2 and HOMO-1. In both processes, the excited molecule decays to the electronic grand state from the $^1\pi\pi^*$ state rather than the $^1n\pi^*$ state. The simulation shows that the lifetime of the $^1n\pi^*$ state is 630 fs in the first excitation and 1120 fs in the second one, compared to the experimental observations of 750 and 1000 fs,[12−14] respectively. On the basis of these simulation results, we propose that the difference in the experimentally observed lifetimes of the $^1n\pi^*$ state at the different excitations is associated with the altered decay pathways developed. This interpretation is different from the currently accepted explanation that the changes in the lifetime of the electronically excited states result from the excitations to different vibrational-excited states.[23−29]

Acknowledgment. This work is supported by the National Natural Science Foundation of China (no. 20773168), Chongqing Natural Science Foundation (no. 3006BB2367), and Chongqing Education Committee Science Technology Project (no. KJ070506). Acknowledgment is also made to the donors of The American Chemical Society Petroleum Research Fund for support of this research at Nicholls State University.

References and Notes

(1) Crespo-Hernández, C. E.; Cohen, B.; Hare, P. M.; Kohler, B. *Chem. Rev.* **2004**, *104*, 1977.
(2) Callis, P. R. *Annu. Rev. Phys. Chem.* **1983**, *34*, 329.
(3) Marian, C.; Nolting, D.; Weinkauf, R. *Phys. Chem. Chem. Phys.* **2005**, *7*, 3306.
(4) Kim, N. J.; Jeong, G.; Kim, Y. S.; Sung, J.; Kim, S. K.; Park, Y. D. *J. Chem. Phys.* **2000**, *113*, 10051.
(5) Plützer, C.; Nir, E.; de Vries, M. S.; Kleinermanns, K. *Phys. Chem. Chem. Phys.* **2001**, *3*, 5466.
(6) Nir, E.; Plützer, C.; Kleinermanns, K.; de Vries, M. S. *Eur. Phys. J.D.* **2002**, *20*, 317.
(7) Plützer, C.; Kleinermanns, K. *Phys. Chem. Chem. Phys.* **2002**, *4*, 4877.
(8) Kim, N. J.; Kang, H.; Park, Y. D.; Kim, S. K. *Phys. Chem. Chem. Phys.* **2004**, *6*, 2802.
(9) Kang, H.; Lee, K. T.; Jung, B.; Ko, Y. J.; Kim, S. K. *J. Am. Chem. Soc.* **2002**, *124*, 12958.
(10) Kang, H.; Jung, B.; Kim, S. K. *J. Chem. Phys.* **2003**, *118*, 6717.
(11) Canuel, C.; Mons, M.; Piuzzi, F.; Tardivel, B.; Dimicoli, I.; Elhanine, M. *J. Chem. Phys.* **2005**, *122*, 074316.
(12) Ullrich, S.; Schultz, T.; Zgierski, M. Z.; Stolow, A. *Phys. Chem. Chem. Phys.* **2004**, *6*, 2796.
(13) Ullrich, S.; Schultz, T.; Zgierski, M. Z.; Stolow, A. *J. Am. Chem. Soc.* **2004**, *126*, 2262.
(14) Samoylova, E.; Lippert, H.; Ullrich, S.; Hertel, I. V.; Radloff, W.; Schultz, T. *J. Am. Chem. Soc.* **2005**, *127*, 1782.
(15) Seefeld, K. A.; Plützer, C.; Löwenich, D.; Häber, T.; Linder, R.; Kleinermanns, K.; Tatchen, J.; Marian, C. M. *Phys. Chem. Chem. Phys.* **2005**, *7*, 3021.
(16) Marian, C. M. *J. Chem. Phys.* **2005**, *122*, 104314.
(17) Fülscher, M. P.; Serrano-Andres, L.; Roos, B. O. *J. Am. Chem. Soc.* **1997**, *119*, 6168.
(18) Broos, A.; Holmen, A. *J. Phys. Chem. A* **1997**, *101*, 3589.
(19) Broos, A. *J. Phys. Chem. A* **1998**, *102*, 526.
(20) Mennucci, B.; Toniolo, A.; Tomasi, J. *J. Phys. Chem. A* **2001**, *105*, 4749.
(21) Salter, L. M.; Chaban, G. M. *J. Phys. Chem. A* **2002**, *106*, 4521.
(22) Lim, E. C. *J. Phys. Chem.* **1986**, *90*, 6770.
(23) Perun, S.; Sobolewski, A. L.; Domcke, W. *Chem. Phys.* **2005**, *313*, 107.
(24) Perun, S.; Sobolewski, A. L.; Domcke, W. *J. Am. Chem. Soc.* **2005**, *127*, 6257.
(25) Chen, H.; Li, S. J. *Phys. Chem. A* **2005**, *109*, 8443.
(26) Blancafort, L. *J. Am. Chem. Soc.* **2006**, *128*, 210.
(27) Serrano-Andrés, L.; Merchán, M.; Borin, A. C. *Proc. Natl. Acad. Sci. U.S.A.* **2006**, *103*, 8691.
(28) Zgierski, M. Z.; Patchkovskii, S.; Lim, E. C. *Can. J. Chem.* **2007**, *85*, 124.
(29) Rachofsky, E. L.; Ross, J. B. A.; Krauss, M.; Osman, R. *J. Phys. Chem. A* **2001**, *105*, 190.
(30) Dou, Y.; Torralva, B. R.; Allen, R. E. *J. Mod. Optics.* **2003**, *50*, 2615.
(31) Dou, Y.; Torralva, B. R.; Allen, R. E. *Chem. Phys. Lett.* **1998**, *378*, 323.
(32) Allen, R. E.; Dumitrica, T.; Torralva, B. R. In *Ultrafast Physical Processes in Semiconductors*; Tsen, K. T. , Ed.; Academic Press: New York, 2001; Chapter 7.
(33) Graf, M.; Vogl, P. *Phys. Rev. B.* **1995**, *51*, 4940.
(34) Boykin, T. B.; Bowen, R. C.; Klimeck, G. *Phys. Rev. B.* **2001**, *63*, 245314.
(35) Torralva, B.; Niehaus, T. A.; Elstner, M.; Suhai, S.; Frauenheim, Th.; Allen, R. E. *Phys. Rev. B* **2001**, *64*, 153105.
(36) Hertel, I. V.; Laarmann, T.; Schulz, C. P. *Adv. Mol. Opt. Phys.* **2005**, *50*, 219.
(37) Dou, Y.; Lei, Y.; Li, A.; Wen, Z.; Torralva, B. R.; Lo, G. V.; Allen, R. E. *J. Phys. Chem. A* **2007**, *111*, 1133.
(38) Pedersen, S.; Herek, J. L.; Zewail, A. H. *Science* **1994**, *266*, 1359.
(39) Dou, Y.; Allen, R. E. *J. Chem. Phys.* **2003**, *119*, 10658.
(40) Bearpark, M. J.; Bernardi, F.; Clifford, S.; Olivucci, M.; Robb, A.; Vreven, T. *J. Phys. Chem. A* **1997**, *101*, 3841.
(41) Porezag, D.; Frauenheim, Th.; Köhler, Th,; Seifert, D.; Kaschner, R. *Phys. Rev. B* **1995**, *51*, 12947.
(42) Born, M.; Oppenheimer, J. R. *Ann. Phys.* **1927**, *84*, 457.
(43) Born, M.; Huang, K. In *The Dynamical Theory of Crystal Lattices*; Oxford University Press: London, 1954.
(44) Teller, E. *J. Phys. Chem.* **1937**, *41*, 109.

(45) In *Conical Intersections: Electronic Structure, Dynamics, and Spectoscopy*; Domcke, W., Eds.;World Scientific: Singapore, 2004.
(46) M, Baer. *Beyond Born-Oppenheimer: Electronic Nonadiabatic Coupling Terms and Conical Intersections*; Wiley Interscience: Hoboken, 2006.
(47) Levine, B. G.; Martínez, T. J. *Annu. Rev. Phys. Chem.* **2007**, *58*, 613.
(48) Toniolo, A.; Levine, B.; Thompson, A. L.; Quenneville, J.; Ben-Nun, M.; Owens, J.; Olsen, S.; Manohar, L.; Martinez, T. J. In *Computational methods in organic photochemistry*; Kutateladze, A. , Ed.; Marcel-Dekker: New York, 2005.

JP802483B